

High-Electron-Affinity Oxide V₂O₅ Enhances Surface Transfer Doping On Hydrogen-Terminated Diamond

Kaijian Xing,¹ Sa Zhang,² Alexander Tsai,³ Haiyan Xiao,^{*, 2} Daniel L. Creedon,³ Steve A.

Yianni,¹ Jeffrey C. McCallum,³ Christopher I. Pakes^{*, 1} and Dong-Chen Qi^{*, 1, 4, 5}

* Corresponding author: Haiyan Xiao, Christopher I. Pakes, Dong-Chen Qi

¹ Department of Chemistry and Physics, La Trobe Institute for Molecular Science, La Trobe University, Bundoora, Victoria 3086, Australia

² School of Physics, University of Electronic Science and Technology of China, Chengdu 610054, China

³ School of Physics, The University of Melbourne, Victoria 3010, Australia

⁴ Centre for Materials Science, Queensland University of Technology, Brisbane, Queensland 4001, Australia

⁵ School of Chemistry and Physics, Queensland University of Technology, Brisbane, Queensland 4001, Australia

Abstract:

Diamond exhibits many desirable properties that could benefit the development of future carbon-based electronic devices. Its hydrogen-terminated surface, in conjunction with a suitable surface acceptor, develops a two-dimensional (2D) *p*-type surface conductivity through the surface transfer doping mechanism which can then be harvested for constructing functional devices. In this study, we have revisited the surface transfer doping of diamond by a high electron affinity (EA) transition metal oxide, V₂O₅. Through a combination of *in-situ* electrical measurements, Hall effect measurements and first-principles density functional theory (DFT) calculations, we explicitly show the intrinsic surface transfer doping behavior of V₂O₅, with doping performance superior to other competing TMOs such as MoO₃. The metallic

surface conduction of diamond induced by V_2O_5 is persistent down to 250 mK; this when coupled with the high hole density exceeding $7 \times 10^{13} \text{ cm}^{-2}$ offers a promising platform for the development of advanced diamond surface electronics exploiting many interesting quantum transport properties of the 2D hole layer of diamond.

Keywords: hydrogen-terminated diamond, vanadium pentoxide, surface transfer doping, DFT

1 Introduction

Diamond is an ultra-wide bandgap, third generation semiconductor material with great promise for building high-power high-frequency electronic devices by harnessing its outstanding intrinsic materials properties, such as high breakdown voltage (over 10 MV/cm), high intrinsic carrier mobility ($4500 \text{ cm}^2/\text{Vs}$ for electrons and $3800 \text{ cm}^2/\text{Vs}$ for holes), and exceptionally high thermal conductivity (22 W/cm K) [1]. Though intrinsic diamond is a bona fide insulator, it is possible to induce a *p*-type surface conductivity (SC) by terminating the diamond surface with hydrogen and exposing to suitable surface acceptors, including air-induced adsorbates. This represents an alternative pathway to constructing diamond-based electronic devices without having to introduce substitutional dopants into the diamond bulk lattice which tends to be problematic [2-4]. Developments based on this surface transfer doping strategy have yielded diamond surface electronic devices including high-performance field-effect transistors (FETs) with drain currents up to 1.3 A/mm [5], and a cut-off frequency up to 53 GHz [6]. However, the poor thermal stability of the SC associated with the volatility of atmospheric adsorbates that originally act as surface acceptors in these devices, has greatly hampered further device development for practical applications. As a result, it is imperative to explore more robust solid-state surface acceptors for achieving high-stability SC on diamond [7-9].

Recently, high electron affinity (EA) transition metal oxides (TMOs), including MoO_3 , V_2O_5 , WO_3 and ReO_3 , were reported as superior alternatives comparing to atmospheric adsorbates [10-17]. Both MoO_3 and V_2O_5 in particular have been reported to be superior surface acceptors in terms of extremely high hole density exceeding $1 \times 10^{14} \text{ cm}^{-2}$ [11] and excellent thermal stability up to 300 °C [12, 13, 15]. In addition, these two TMOs have been also demonstrated as gate dielectric layers as well as a surface acceptor layer to reduce the device access resistance in hydrogen-terminated diamond MOSFETs [18, 19, 20], promising a great potential in diamond device applications by using the TMO doping strategy. More recently, MoO_3 has been systematically studied by a combination of *in-situ* electrical characterization and first-principles density functional theory (DFT) calculations [17]. It not only rules out the confounding effects of atmospheric dopants by *in-situ* measurement, but also shows a MoO_3 -induced metallic conduction down to cryogenic temperature regime [17], opening a way for investigating the possible quantum effects, such as spin-orbit interaction reported in air-doped diamond systems [21, 22]. However, no comparable study on V_2O_5 transfer doping has been carried out.

In this work, we have studied the intrinsic surface transfer doping capacity of V_2O_5 using a combination of *in-situ* and variable temperature electrical characterization, as well as first-principles calculations. We show that the very initial V_2O_5 deposition already yields a dramatic decrease in sheet resistance of diamond surface during the *in-situ* four-point-probe measurements. The surface transfer doping process between V_2O_5 and the hydrogen-terminated diamond surface can be modelled successfully by considering the Fermi-Dirac statistics and charge neutrality across the interface. Variable-temperature Hall effect measurements from 300 K down to 250 mK further reveals metallic conduction of the 2D hole

layer induced by V_2O_5 transfer doping. The charge separation at the interface with V_2O_5 capping and its impact on the electronic structures were explored by DFT calculation as well.

2 Experimental

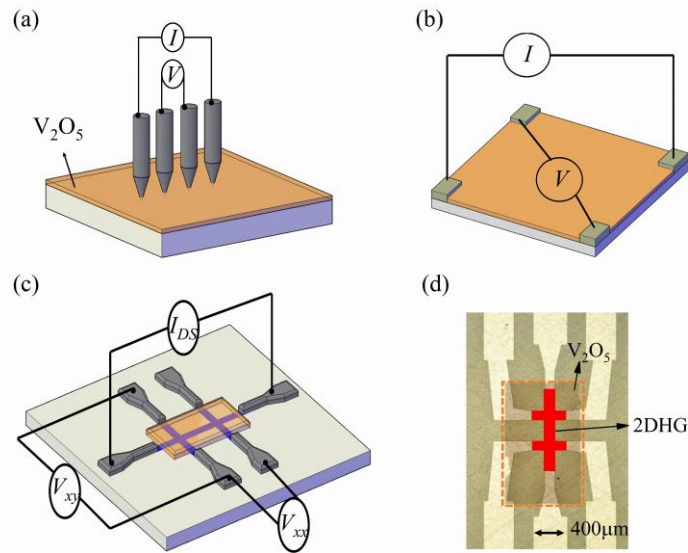


Figure 1. Schematic representation showing electrical set up of : (a) the four-point-probe measurement, (b) the van de Pauw (VdP) measurement, (c) Hall bar measurement on V_2O_5 doped diamond devices. (d) optical image of the V_2O_5 doped hall bar device. The orange dashed box outlines the V_2O_5 layer while the red hall bar structure represents the hydrogen-terminated region.

2.1 In-situ four-point probe measurement

Commercial IIa (100) single crystal diamonds were terminated in a hydrogen plasma reactor (*Astex system*) operating at a power of 1500 W (power density $\sim 5.6 \text{ W/cm}^3$) with a substrate temperature set to 850 °C for 10 mins to achieve the hydrogen-terminated 2×1 reconstructed surface. *In-situ* characterisation of the sheet resistance of hydrogen-terminated diamond as a function of V_2O_5 coverage was carried out by using a four-point probe (*Jandel*) in a custom-built ultra-high vacuum system with a base pressure of 3×10^{-10} mbar. Firstly, the hydrogen-

terminated diamond was annealed at 400 °C for 30 minutes, which completely desorbs atmospheric surface adsorbates while keeping the hydrogen-termination intact [7, 10, 12, 17]. V_2O_5 was then thermally deposited on the pristine hydrogen-terminated diamond surface using a standard Knudsen cell at 775 °C with the deposition rate of 0.15 Å/minute measured by a quartz crystal microbalance. The nominal thickness of V_2O_5 layer was calibrated by using a correction factor independently determined by spectroscopic ellipsometry (*J.A. Woollam M-2000DI*). The sheet resistance was measured *in-situ* as a function of V_2O_5 thickness using the four-point probe as shown in Figure 1a. After pressing the probes onto the sample directly, the *I-V* measurements were carried out using a Keithley 2450 sourcemeter. The calculation of the sheet resistance has been geometrically corrected to account for sample dimensions and probe spacing [23]. After the *in-situ* measurements, van de Pauw (VdP) Ohmic contacts were fabricated on the corners of the sample using conductivity epoxy, as shown in Figure 1b, to measure the hole density of the V_2O_5 -doped diamond. Before the epoxy formation, V_2O_5 on the corners of the diamond was scratched off to ensure a direct contact between the epoxy contacts and the diamond surface.

2.2 Hall bar device fabrication and temperature-dependent Hall effect measurements

Hall bar devices with a width/length of 40 μm /200 μm were fabricated on the hydrogen-terminated diamond following standard photolithographic techniques and lift-off processes reported elsewhere [21, 22]. Hall bar active regions were defined with a protective layer of photoresist while the uncovered regions of the sample were exposed to a 50 W oxygen plasma at room temperature and rendered insulating for device isolation. The metal-contact regions contained a mixture of hydrogen- and oxygen-terminated surface aiming to enhance the adhesion between metal and diamond surface. 100 nm Pd was then deposited on the diamond using an electron beam evaporator to form excellent Ohmic contacts which persists even at

cryogenic temperature [24]. As shown in Figure 1d, 20 nm V_2O_5 was thermally deposited on the active hall-bar regions through a shadow mask in a custom-built ultra-high-vacuum (UHV) system with a base pressure of 3×10^{-10} mbar after the 400 °C pre-annealing process.

Hall effect measurements of the diamond devices were performed from 0.25 K to 20 K using a Leiden Cryogenics dry dilution refrigerator with a 9-1-1 T superconducting vector magnet. A separate Hall effect measurement system (*Janis*) with a 0.7 T coil magnet was utilized to characterise the electrical transport properties of both the hall-bar devices (Figure 1c) and VdP device (Figure 1b) at room temperature for reference. A standard low-frequency AC lock-in amplifiers (Stanford SR830) was employed in the Leiden Cryogenics dry dilution refrigerator to minimize noise, while a Keithley 2450 Sourcemeter was employed for the *Janis* system to achieve DC measurements of V_{xx} . The Hall voltage V_{xy} was simultaneously measured using an Agilent 34410A multimeter to determine the transverse resistance, R_{xy} .

2.4 Computational Details

In the present work, first-principles calculations within the DFT framework were carried out. All calculations were performed using the Vienna Ab-initio Simulation Package (VASP) code based on the projector augmented wave method [25, 26]. The exchange-correlation effects were treated using the Perdew-Burke-Ernzerhof functional under the generalized gradient approximation (GGA) [27]. The on-site Coulomb interaction presented in 3d states of transition-metal ions was corrected by the DFT + U ($U = 3$ eV) method [28, 29]. A cut-off energy of 550 eV for the plane wave basis set and a $4 \times 4 \times 1$ Monkhorst-Pack k -mesh for Brillouin-zone integrations were used for structural relaxation. The convergence criteria for total energies and forces were 10^{-4} eV and 10^{-3} eV/Å, respectively. The slab models, in which one slab consisting of 10 monolayers of diamond and two layers of H along [001] direction (including 240 C atoms and 48 H atoms) and a vacuum region of 20 Å separating the

periodically repeated slabs, were employed in the calculations. The position of the V_2O_5 molecule and the atoms in the top four layers were fully relaxed and the remaining atoms were fixed during the structural optimization.

3 Results and Discussion

3.1 In-situ four-point probe measurement and VdP Hall effect measurement

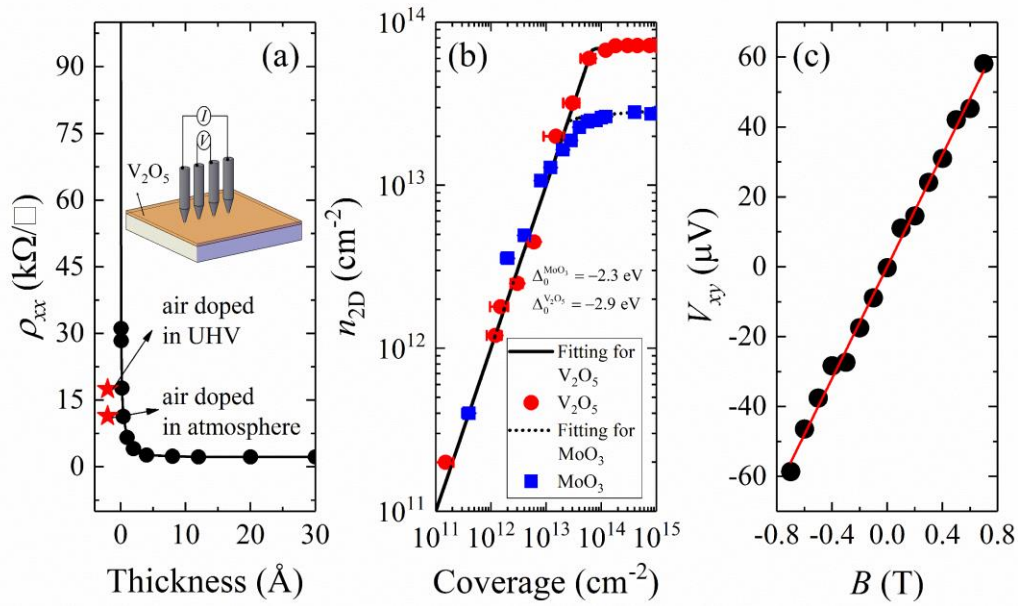


Figure 2 (a) Sheet resistance of hydrogen-terminated diamond surface is observed to decrease with increasing V_2O_5 thickness. The initial resistance values in atmosphere and in UHV are labelled with red stars. (b) Experimental and theoretical hole density values as a function of TMO (V_2O_5 and MoO_3) coverage. The solid red circles represent the experimental data for the V_2O_5 -doped device. Hole densities for the MoO_3 -doped device taken from ref. [17] (solid blue squares) are plotted together for comparison. The solid and dashed lines correspond to the best fits using Eq. 6 with an initial activation energy (Δ_0) of 2.85 ± 0.1 eV for V_2O_5 and 2.3 ± 0.1 eV for MoO_3 , respectively. (c) The experimental Hall voltage V_{xy} is seen to vary with applied magnetic field with a linear fit shown in red.

The hydrogen-terminated diamond was measured, by four-point probe, to have an initial sheet resistance of $11.44 \text{ k}\Omega/\square$ in atmosphere, which is consistent with values reported for the air-induced, naturally occurring SC of diamond in literature. After placing in UHV for 24 hours, the sheet resistance slowly increased to $17.51 \text{ k}\Omega/\square$ due to partial desorption of the surface adsorbates, as shown in Figure 2a. Then we annealed the hydrogen-terminated diamond at 400°C for 30 minutes to completely remove the residual surface adsorbates. The removal was verified by the *in-situ* four-point probe measurement which yielded a sheet resistance that exceeded the limit of the Keithley Sourcemeter. Upon V_2O_5 deposition, the sheet resistance of diamond experienced a significant reduction and saturated at $2.23 \text{ k}\Omega/\square$ when the thickness exceeded 8 \AA , which is among the lowest reported values on hydrogen-terminated (100) diamond when compared with other TMOs, such as MoO_3 [10, 11, 13, 15], WO_3 [14] and Nb_2O_5 [14]. The drastic decrease of sheet resistance at very low V_2O_5 coverage is consistent with photoemission measurements which revealed a strong upward band bending at the surface of the diamond with a deposited V_2O_5 thickness as low as 1 \AA [12]. The sheet resistance of the V_2O_5 -doped hydrogen-terminated diamond sample (after final deposition) was also independently measured *ex-situ* in a VdP configuration to be $2.04 \text{ k}\Omega/\square$ by using Eq. (S0) (see Supplementary Material for details) [30], which shows excellent agreement with the *in-situ* four-point-probe measurement and additionally indicates that the V_2O_5 induced surface transfer doping is stable in air. The VdP device also allowed us to determine the hole density (n_{2D}) through the Hall-effect measurements. Figure 2c shows the Hall voltage V_{xy} as a function of magnetic field B from which n_{2D} is calculated to be $7.8 \times 10^{13} \text{ cm}^{-2}$ using $n_{2D} = I/(q \times V_{xy}/B)$, in which I , q , V_{xy} and B are the drain current, elementary charge, Hall voltage, and magnetic field, respectively. This hole density is amongst the highest reported values achieved for V_2O_5 doped (100) hydrogen-terminated diamond [12, 13, 15, 31]. In addition, the hole mobility is calculated as $39 \text{ cm}^2/\text{V}\cdot\text{s}$, which is considered relatively high at this hole

density range when compared with previous studies. The discrepancy in hole mobility might be caused by the difference in diamond surface roughness or long-range potential fluctuations associated with hydrogen-termination quality [32, 33], which is still a subject of debate.

The sheet resistance measured by the *in-situ* four-point probe can be related to the hole density as follows:

$$\rho_{xx} = 1 / (q \cdot \mu \cdot n_{2D}) \quad \text{Eq.(1)}$$

where μ and ρ_{xx} represent the carrier mobility and sheet resistance, respectively. As the carrier mobility typically decreases with increasing hole density, assuming a constant hole mobility will result in an overestimation of the hole density at low V_2O_5 coverage. In Figure S2a, the mobility was plotted as a function of $\log_{10}(n_{2D})$ based on an independent Hall effect dataset sampled from a large range of air-doped diamond samples, resulting in an empirical relationship of $\log_{10}(n_{2D})$, in which A and B are the fitting parameters. Thus, an empirical relationship between ρ_{xx} and n_{2D} can be obtained as (also see Figure S2b):

$$\rho_{xx} = \frac{1}{q \cdot [A \cdot \log_{10}(n_{2D}) + B] \cdot n_{2D}} \quad \text{Eq. (2)},$$

which allows us to estimate the induced hole density as a function of V_2O_5 coverage as shown in Figure 2b. It is clear that n_{2D} steeply increases at low V_2O_5 coverage and eventually saturates at high coverage with a final hole density of $7.2 \times 10^{13} \text{ cm}^{-2}$, which is consistent with the VdP Hall measurement results. Such a high hole density demonstrates that V_2O_5 is a superior surface acceptor when compared to other TMOs such as MoO_3 [17], as the saturated hole density is more than two times higher, as shown in Figure 2b. The dependence of carrier concentration induced by surface transfer doping on the coverage of surface acceptors can be modelled by considering Fermi-Dirac statistics and charge neutrality across the interface [2, 8]. The Fermi-Dirac probability governs the occupation of the acceptors in the following equation:

$$n_{2D} = N_{A^-} = N_A \cdot \frac{1}{\exp\left[\left(E_C^{V_2O_5} - E_F\right) / kT\right] + 1} \quad \text{Eq.(3)}$$

in which n_{2D} is the induced hole density in diamond. N_A and N_{A^-} are the total areal density for V_2O_5 and negatively charged V_2O_5 acceptors, respectively. The Boltzmann constant and temperature are represented by k and T respectively, while $E_C^{V_2O_5}$ and E_F refer to the conduction band edge of V_2O_5 and Fermi-energy level, respectively. The energy term $(E_C^{V_2O_5} - E_F)$ in the equation above can be rewritten by relating to the other two energy terms Δ and u_s as:

$$E_C^{V_2O_5} - E_F = \left(E_C^{V_2O_5} - E_V^{\text{Diamond}}\right) + \left(E_V^{\text{Diamond}} - E_F\right) = \Delta + u_s(n_{2D}) \quad \text{Eq.(4)}$$

where Δ is the energy difference between $E_C^{V_2O_5}$ and the valence band edge of diamond at the surface E_V^{Diamond} and is referred to as the acceptor energy. $u_s(n_{2D})$ is defined as the energy offset between the E_V^{Diamond} and the Fermi energy at the surface; it depends on the hole density and is modulated by the upward band bending at the diamond surface (more details in SI).

The spatial separation between electrons trapped in the V_2O_5 and the holes accumulated at the diamond surface due to the surface transfer doping creates an induced interfacial dipole, $(\Delta\Phi)$, that modifies the band alignment across the interface by lifting the vacuum level of the surface acceptors. Therefore, we can rewrite the acceptor energy as $\Delta = \Delta_0 + \Delta\Phi$, in which $\Delta_0 = IP_{\text{Diamond}} - EA_{V_2O_5}$ is the initial acceptor energy determined by the difference between the ionisation energy of diamond and the EA of V_2O_5 . Based on a simple electrostatic capacitor model, the magnitude of the interface dipole can be modeled as $\Delta\Phi(n_{2D}) = q^2 \times n_{2D} / C_{\square}$, in C_{\square} which is calculated to be $3.23 \times 10^{13} \text{ e/cm}^2 \cdot \text{V}$ by assuming relative permittivity of 5.7 and a separation distance of 0.3 nm obtained from DFT calculation. Consequently, the Eq. (4) can be rewritten as:

$$E_C^{V_2O_5} - E_F = \Delta_0 + q^2 \cdot n_{2D} / C_{\square} + u_s(n_{2D}) \quad \text{Eq.(5)}$$

Substituting Eq. (5) into Eq. (3) further yields the relationship between n_{2D} and N_A :

$$n_{2D} = N_{A^-} = N_A \cdot \frac{1}{\exp\left\{\left[\Delta_0 + q^2 \cdot n_{2D} / C_{\square} + u_s(n_{2D})\right] / kT\right\} + 1} \quad \text{Eq.(6)}$$

which allows us to quantitatively calculate the hole density at the diamond surface for a given values of V_2O_5 coverage N_A .

In Figure 2b, we use Eq. (6) to fit the hole density as a function of V_2O_5 coverage by considering Δ_0 as the only free fitting parameter. The black solid line corresponding to the hole density calculated with an initial activation energy of $\Delta_0^{V_2O_5} = -2.9 \pm 0.1$ eV fits the experimental data reasonably well. The extracted initial activation energy of V_2O_5 -doped diamond is more negative than the one for MoO_3 reported earlier by us [17], corroborating the better doping efficiency of V_2O_5 on hydrogen-terminated diamond. The obtained activation energy $\Delta_0^{V_2O_5}$ yields an EA of 7.1 ± 0.1 eV for V_2O_5 by adopting an IP of 4.2 eV for diamond, which is consistent with the literature [34]; this places the conduction band edge of V_2O_5 2.9 eV *below* the VBM of the diamond.

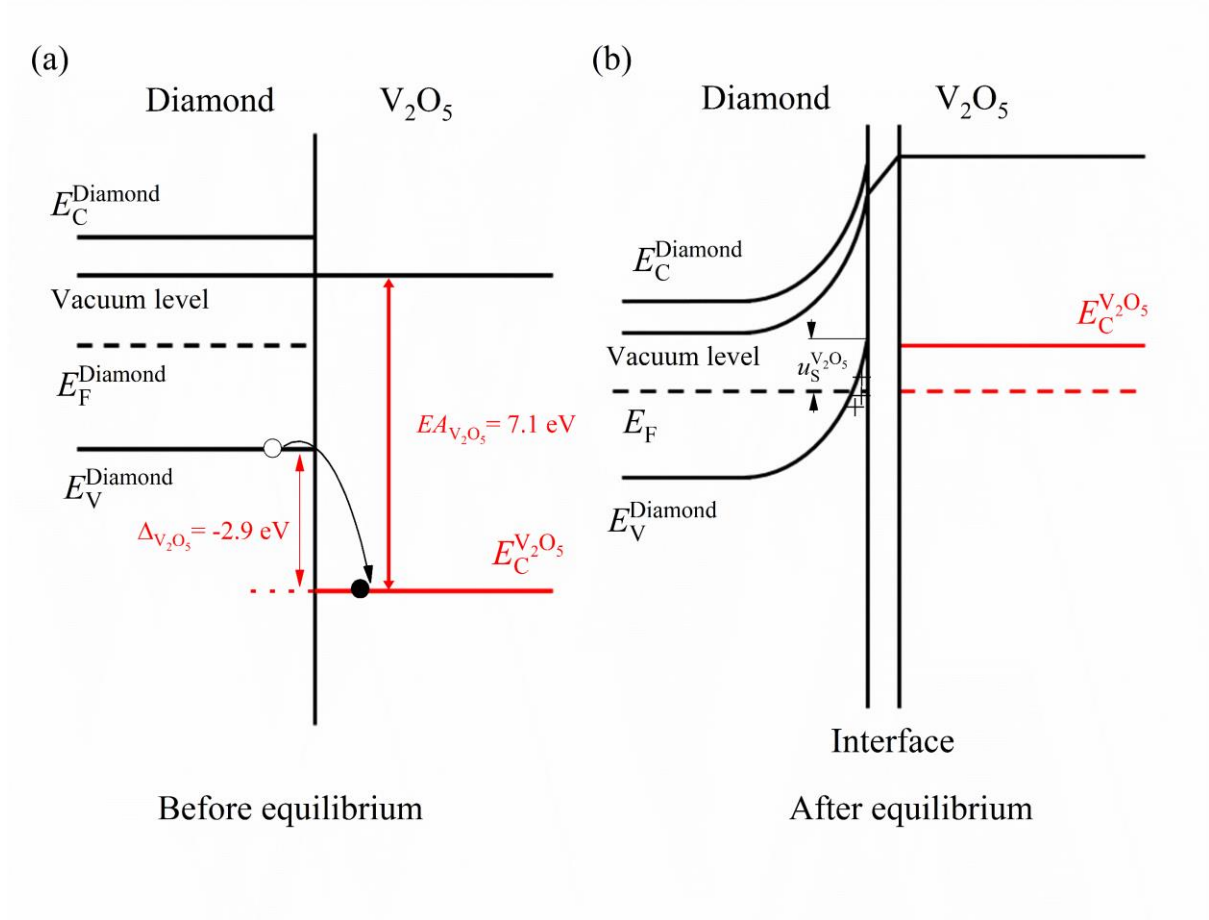


Figure 3 Schematic energy band diagram before (a) and after (b) surface transfer doping using V_2O_5 as surface acceptors.

Figure 3 schematically represents the energy level alignment before and after the surface transfer doping between V_2O_5 and hydrogen-terminated diamond. In Figure 3a, the conduction band minimum (CBM) of V_2O_5 lies approximate 2.9 eV below the hydrogen-terminated diamond valence band maximum (VBM) due to the very high EA of V_2O_5 relative to the very low ionization energy of hydrogen-terminated diamond as a result of its unique true negative EA, suggesting that the spontaneous transfer of electrons from the diamond surface to V_2O_5 is energetically favorable. The charge transfer process reaches thermodynamic equilibrium when the Fermi level on each side of the interface is aligned, as shown in Figure 3b. Due to the strong upward band bending at the diamond side, the Fermi level goes below the VBM of diamond,

giving rise to a hole accumulation layer strongly confined at the diamond surface [12]. The higher EA of V_2O_5 and hence more negative initial activation energy as compared to other TMOs such as MoO_3 is consistent with its better doping yield, as also demonstrated by other *ex-situ* transport measurements [13].

3.2 Variable-temperature transport measurement

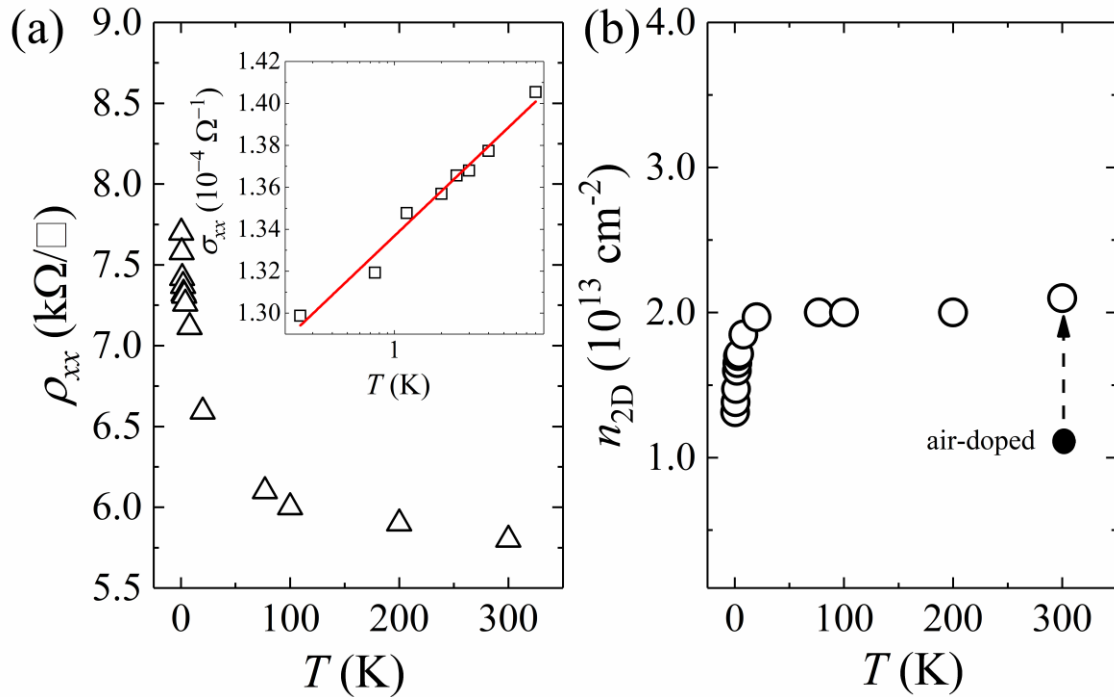


Figure 4 Temperature-dependent transport properties of V_2O_5 doped Hall bar devices. (a) Longitudinal sheet resistance as a function of temperature from 250 mK to 300 K. Inset in (a) depicts the linear relationship between the sheet conductivity and temperature in the same range but with a log scale. (b) Hole density as function of temperature from 250 mK to 300 K. The solid circle represents the air-induce hole density.

After annealing the pristine air-doped Hall bar diamond devices followed by an *in-situ* deposition of 10 nm of V_2O_5 on the active regions, results in a significant increase in hole density from $1.2 \times 10^{13} \text{ cm}^{-2}$ to $2.1 \times 10^{13} \text{ cm}^{-2}$ at 300 K, indicating the superiority of V_2O_5 for

surface transfer doping efficiency over the air-doped strategy, which is consistent with the *in-situ* measurement results. It is worth noting that the hole density extracted from the Hall bar device is lower than the one extracted from the VdP device. In addition to the well-known overestimation of VdP measurements [35], this discrepancy might be caused by potential photoresist residues left from the photolithographic process during the fabrication of Hall bar devices, which could affect the local hole density by interfering with the surface transfer doping process [36]. The negative activation energy of the V_2O_5 surface acceptors owing to the large EA implies that no thermal activation energy is required to initiate the surface transfer doping process, thereby preventing carrier-freeze out at cryogenic temperature. Figure 4 shows the temperature-dependent Hall effect measurements of the V_2O_5 (10 nm) doped diamond Hall-bar device from 300 K down to 250 mK. The V_2O_5 doped Hall-bar device exhibits almost no temperature dependence both in terms of hole density and sheet resistance from 300 K to 20 K, indicating a metallic rather than a thermally activated conduction in the 2D hole channel induced by V_2O_5 doping. Further cooling down to 250 mK leads to a slight increase in sheet resistance from $6.6 \text{ k}\Omega/\square$ to $7.7 \text{ k}\Omega/\square$, corresponding to a reduction in hole density from $1.97 \times 10^{13} \text{ cm}^{-2}$ to $1.32 \times 10^{13} \text{ cm}^{-2}$. The sheet conductivity as shown in the inset of Figure 4a follows the $\log_{10}(T)$ relationship from 20 K to 250 mK. The logarithmic temperature dependence rather than exponential is strong evidence for metallic behavior of V_2O_5 induced SC at diamond surface. A similar temperature dependence has also been observed in the air-induced, ionic-liquid gated SC and MoO_3 -induced SC in diamond [17, 21, 22]. The reduction in diamond surface conductivity (and hole density) is caused by quantum corrections to the classical Drude conductivity, such as hole-hole interaction and phase coherence backscattering [37]. Consequently, the diamond surface metallic condition down to 250 mK can be realised by V_2O_5 surface transfer doping strategy.

3.3 DFT Calculation

DFT calculations allow us to gain an atomic level understanding of the interaction between V_2O_5 surface acceptors and the hydrogen-terminated diamond surface. The modified adsorption configurations of V_2O_5 molecules on hydrogen-terminated diamond surface was firstly studied by calculating the adsorption energy (ΔE) of V_2O_5 on the diamond surface for different possible configurations:

$$\Delta E = E_{V_2O_5/H\text{-diamond}} - E_{V_2O_5} - E_{H\text{-diamond}} \quad \text{Eq. (9)}$$

where $E_{H\text{-diamond}}$ and $E_{V_2O_5/H\text{-diamond}}$ are the total energies of the relaxed hydrogen-terminated diamond surface before and after MoO_3 adsorption. $E_{V_2O_5}$ is the total energy of an isolated V_2O_5 molecule [38]. In this work, we considered several possible adsorptions configurations of V_2O_5 as shown in Figure S3. According to the optimized structure for the possible adsorptions configurations, the lowest adsorption energy of -0.66 eV for Parallel A configuration can be determined as the most favorable adsorption configuration (More details in SI). Thus we selected Parallel A to explore the surface transfer doping process between V_2O_5 and hydrogen-terminated diamond in detail. The charge density difference ($\Delta\rho$) between V_2O_5 molecules and the hydrogen-terminated diamond surface is illustrated in Figure 5a. The $\Delta\rho$ can be calculated as $\Delta\rho = \rho_{V_2O_5/H\text{-diamond}} - \rho_{V_2O_5} - \rho_{H\text{-diamond}}$, where $\rho_{V_2O_5}$ and $\rho_{H\text{-diamond}}$ are the charge densities of isolated V_2O_5 molecules and the pristine hydrogen-terminated diamond surface. $\rho_{V_2O_5/H\text{-diamond}}$ represents the charge density of the V_2O_5 adsorbed hydrogen-terminated diamond surface [39]. In Figure 5a, the yellow regions represent the electron accumulation and the blue regions represent the hole accumulation. This clearly shows the charge transfer between V_2O_5 and hydrogen-terminated diamond surface, leaving a hole accumulation layer on diamond surface and electron accumulation around the O atoms in the V_2O_5 molecules. The Bader charge population for the pristine and V_2O_5 doped hydrogen-terminated diamond surface was

further evaluated to quantify the amount of hole at diamond surface. It shows that each V_2O_5 molecule extracts 0.41 electrons from the top layer of the diamond surface. The amount of charge transfer for each V_2O_5 molecule is comparable to that calculated for V_2O_5 on II-VI semiconductors (i.e. ZnS, ZnSe), but is notably higher than those for other types of TMO on diamond as predicted by our previous DFT work. For example, Xiang et al. showed that each CrO_3 gains 0.36 electrons from the diamond surface while Xing et al. demonstrated that each MoO_3 gains 0.24 electrons from diamond surface [17, 40]. This places V_2O_5 as a superior surface acceptor among high EA TMOs for surface transfer doping of diamond.

The density of state (DOS) distribution of the hydrogen-terminated diamond surface before and after V_2O_5 adsorption is shown in Figure 5b, which provides insight into the impact of interfacial charge transfer on electronic structures [41]. For the V_2O_5 -doped hydrogen-terminated diamond surface, the Fermi level clearly moves into the top of the diamond valence band, indicating a strong degenerate doping effect and predicting the metallic nature of the *p*-type conduction channel induced by V_2O_5 at diamond surface, which is consistent with the low-temperature Hall effect measurements. Overall the DFT calculations provide strong theoretical support for the interfacial charge transfer process and the superior doping performance of V_2O_5 on hydrogen-terminated diamond.

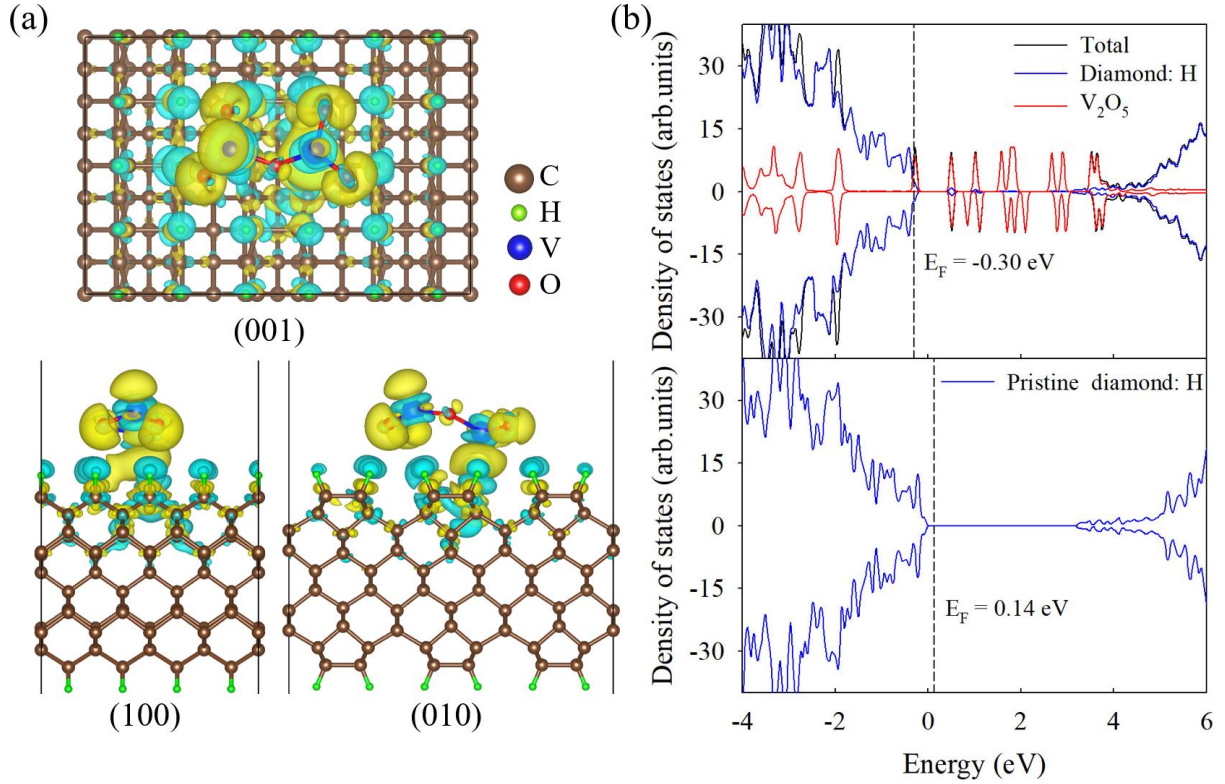


Figure 5. DFT calculations of the V_2O_5 adsorbed hydrogen-terminated diamond surface. (a) Top and side view of charge density differences for the most preferable configuration of V_2O_5 adsorption. The yellow regions represent the electron accumulation and the blue regions represent the hole accumulation. (b) Density of states distribution of V_2O_5 -doped hydrogen-terminated diamond surface and the pristine hydrogen-terminated diamond surface.

4 Conclusions

In summary, V_2O_5 has been demonstrated as a superior surface acceptor to induce *p*-type surface conductivity on hydrogen-terminated diamond (001) surface as verified by a combination study of *in-situ* electrical characterization, variable-temperature Hall effect measurements and DFT calculations. After a low coverage deposition of V_2O_5 , the diamond surface is transformed from insulating to conducting as seen by a dramatic decrease in sheet resistance which eventually saturates at $2.23 \text{ k}\Omega/\square$, corresponding to a high hole density of approximately exceeding $7 \times 10^{13} \text{ cm}^{-2}$. The doping process by V_2O_5 is fully consistent with

the surface transfer doping model employing Fermi-Dirac statistics and charge neutrality, yielding a negative initial activation energy of $-2.85 \text{ eV} \pm 0.1 \text{ eV}$. Consistent with the large negative activation energy, low temperature transport characterisation reveals a prevailing metallic conduction in the V_2O_5 induced hole conducting channel down to 250 mK, manifesting its 2D Fermi liquid nature. The superior surface transfer doping of V_2O_5 is also corroborated by DFT calculations which demonstrates charge transfer across the interface and the degenerate doping effect. This work provides insights into the surface transfer doping of diamond by V_2O_5 , suggesting that this doping strategy could offer an attractive route towards the development of future high-performance diamond surface electronics as well as quantum devices working at cryogenic temperatures.

Supplementary Material

Supplementary Material is available online or from the authors.

Acknowledgments

This work was supported by the Australian Research Council under the Discovery Project (No. DP150101673). D. Q. acknowledges the support of the Australian Research Council (Grant No. FT60100207) and the continued support from the Queensland University of Technology (QUT) through the Centre for Materials Science.

Founding Source

The Australian Research Council (Grant NO. DP150101673) (Grant NO. FT60100207)

Corresponding Authors

Prof. Haiyan Xiao: hy.xiao@uestc.edu.cn; Prof. Christopher I. Pakes: C.pakes@latrobe.edu.au;

Dr. Dong-Chen Qi: dongchen.qi@qut.edu.au

References

- [1] M. Kasu, K. Ueda, Y. Yamauchi, A. Tallaire, T. Makimoto, Diamond-based RF power transistors: Fundamentals and applications, *Diam. Relat. Mater.* 16 (2007) 1010–1015.
- [2] J. Ristein, Surface Transfer Doping of Diamond, *J. Phys. D Appl. Phys.* 39 (2004) 432–437.
- [3] F. Maier, M. Riedel, B. Mantel, J. Ristein, L. Ley, Origin of surface conductivity in diamond, *Phys. Rev. Lett.* 85 (2000) 3472–3475.
- [4] L. Ley, Chapter 4 Surface Conductivity of Diamond, 2009.
- [5] K. Hirama, H. Sato, Y. Harada, H. Yamamoto, M. Kasu, Diamond Field-Effect Transistors with 1.3 A/mm Drain Current Density by Al₂O₃ Passivation Layer, *Jpn. J. Appl. Phys.* 51 (2012) 090112.
- [6] S. Russell, S. Sharabi, A. Tallaire, D.A.J. Moran, RF operation of hydrogen-terminated diamond field effect transistors: A comparative study, *IEEE Trans. Electron Devices.* 62 (2015) 751–756.
- [7] D. Qi, W. Chen, X. Gao, L. Wang, S. Chen, P.L. Kian, A.T.S. Wee, Surface transfer doping of diamond (100) by tetrafluoro- tetracyanoquinodimethane, *J. Am. Chem. Soc.* 129 (2007) 8084–8085.
- [8] P. Strobel, M. Riedel, J. Ristein, L. Ley, Surface transfer doping of diamond by fullerene, *Diam. Relat. Mater.* 430 (2005) 439–441.
- [9] M.T. Edmonds, M. Wanke, A. Tadich, H.M. Vulling, K.J. Rietwyk, P.L. Sharp, C.B. Stark, Y. Smets, A. Schenk, Q.H. Wu, L. Ley, C.I. Pakes, Surface transfer doping of hydrogen-terminated diamond by C₆₀F₄₈: Energy level scheme and doping efficiency, *J. Chem. Phys.* 136 (2012) 124701.
- [10] S.A.O. Russell, L. Cao, D. Qi, A. Tallaire, K.G. Crawford, A.T.S. Wee, D.A.J. Moran, Surface transfer doping of diamond by MoO₃: A combined spectroscopic and Hall measurement study,

- Appl. Phys. Lett. 103 (2013) 202112.
- [11] M. Tordjman, C. Saguy, A. Bolker, R. Kalish, Superior Surface Transfer Doping of Diamond with MoO_3 , Adv. Mater. Interfaces. 1 (2014) 1300155.
 - [12] K.G. Crawford, L. Cao, D. Qi, A. Tallaire, E. Limiti, C. Verona, A.T.S. Wee, D.A.J. Moran, Enhanced surface transfer doping of diamond by V_2O_5 with improved thermal stability, Appl. Phys. Lett. 108 (2016) 042103.
 - [13] C. Verona, W. Ciccognani, S. Colangeli, E. Limiti, M. Marinelli, G. Verona-Rinati, Comparative investigation of surface transfer doping of hydrogen terminated diamond by high electron affinity insulators, J. Appl. Phys. 120 (2016) 025104.
 - [14] M. Tordjman, K. Weinfeld, R. Kalish, Boosting surface charge-transfer doping efficiency and robustness of diamond with WO_3 and ReO_3 , Appl. Phys. Lett. 111 (2017) 111601.
 - [15] K.G. Crawford, D. Qi, J. McGlynn, T.G. Ivanov, P.B. Shah, J. Weil, A. Tallaire, A.Y. Ganin, D.A.J. Moran, Thermally Stable, High Performance Transfer Doping of Diamond using Transition Metal Oxides, Sci. Rep. 8 (2018) 3342.
 - [16] Z. Liu, G. Fang, Y. Wang, Y. Bai, K.-L. Yao, Laser-induced colouration of V_2O_5 , J. Phys. D: Appl. Phys. 33 (2018) 2327–2332.
 - [17] K. Xing, Y. Xiang, M. Jiang, D.L. Creedon, G. Akhgar, S.A. Yianni, H. Xiao, L. Ley, A. Stacey, J.C. McCallum, S. Zhuiykov, C.I. Pakes, D.-C. Qi, MoO_3 induces *p*-type surface conductivity by surface transfer doping in diamond, Appl. Surf. Sci. 509 (2020) 144890.
 - [18] P. Taylor, Y. Chen, C. Hsu, K. Chen, H-Terminated Diamond MISFETs with V_2O_5 as Insulator, IEEE. (2016) 1–4.
 - [19] Z. Ren, J. Zhang, J. Zhang, C. Zhang, S. Xu, Y. Li, Y. Hao, Diamond Field Effect Transistors With MoO_3 Gate Dielectric, IEEE Electron Device Lett. 38 (2017) 786–789.
 - [20] D.A. Macdonald, K.G. Crawford, A. Tallaire, R. Issaoul, D.A.J. Moran, Performance Enhancement of $\text{Al}_2\text{O}_3/\text{H}$ -Diamond MOSFETs Utilizing Vacuum Annealing and V_2O_5 as a Surface Electron Acceptor, IEEE Electron Device Lett. 39 (2018) 1354–1357.
 - [21] M.T. Edmonds, L.H. Willems Van Beveren, O. Klochan, J. Cervenka, K. Ganesan, S. Praver, L. Ley, A.R. Hamilton, C.I. Pakes, Spin-orbit interaction in a two-dimensional hole gas at the

- surface of hydrogenated diamond, *Nano Lett.* 15 (2015) 16–20.
- [22] G. Akhgar, O. Klochan, L.H. Willems Van Beveren, M.T. Edmonds, F. Maier, B.J. Spencer, J.C. McCallum, L. Ley, A.R. Hamilton, C.I. Pakes, Strong and tunable spin-orbit coupling in a two-dimensional hole gas in ionic-liquid gated diamond devices, *Nano Lett.* 16 (2016) 3768–3773.
 - [23] F.M. Smits, Measurement of Sheet Resistivities with Four-Point Probe, *Bell Syst. Tech. Pap.* 37 (1957) 711–718.
 - [24] K. Xing, A. Tsai, S. Rubanov, D.L. Creedon, S.A. Yianni, L. Zhang, W.-C. Hao, J. Zhuang, J.C. McCallum, C.I. Pakes, D.-C. Qi, *Appl. Phys. Lett.* 116 (2020) 111601.
 - [25] G. Kresse, J. Hafner, Ab initio molecular dynamics for liquid metals, *Phys. Rev. B.* 47 (1993) 558–561.
 - [26] C. Payne, N. York, Ab initio iterative minimization techniques, *October.* 64 (1992) 1045–1097.
 - [27] J.P. Perdew, K. Burke, M. Ernzerhof, Generalized gradient approximation made simple, *Phys. Rev. Lett.* 77 (1996) 3865–3868.
 - [28] T. Das, S. Tosoni, G. Pacchioni, Structural and electronic properties of bulk and ultrathin layers of V_2O_5 and MoO_3 , *Comput. Mater. Sci.* 163 (2019) 230–240.
 - [29] S. Zhang, H.Y. Xiao, S.M. Peng, G.X. Yang, Z.J. Liu, X.T. Zu, S. Li, D.J. Singh, L.W. Martin, L. Qiao, Band-Gap Reduction in $(BiCrO_3)_m/(BiFeO_3)_n$ Superlattices: Designing Low-Band-Gap Ferroelectrics, *Phys. Rev. Appl.* 10 (2018) 044004.
 - [30] Z. Yang, H. Peng, W. Wang, T. Liu, Crystallization behavior of poly(ϵ -caprolactone)/layered double hydroxide nanocomposites, *J. Appl. Polym. Sci.* 116 (2010) 2658–2667.
 - [31] Z. Liu, G. Fang, Y. Wang, Y. Bai, K.-L. Yao, Influence of surface crystal-orientation on transfer doping of V_2O_5 /H-terminated diamond, *J. Phys. D. Appl. Phys.* 112 (2018) 181602.
 - [32] K.G. Crawford, A. Tallaire, X. Li, D.A. Macdonald, D. Qi, D.A.J. Moran, The role of hydrogen plasma power on surface roughness and carrier transport in transfer-doped H-diamond, *Diam. Relat. Mater.* 84 (2018) 48–54.
 - [33] R. Peterson, M. Malakoutian, X. Xu, C. Chapin, S. Chowdhury, D.G. Senesky, Analysis of the Mobility-Limiting Mechanisms of the Two-Dimensional Hole Gas on Hydrogen-Terminated

- Diamond. arXiv:2003.08007v1 [physics.app-ph] (2020) 1–11.
- [34] A. Kuruvila, P.R. Kidambi, J. Kling, J.B. Wagner, J. Robertson, S. Hofmann, J. Meyer, Organic light emitting diodes with environmentally and thermally stable doped graphene electrodes, *J. Mater. Chem. C* 2 (2014) 6940–6945.
 - [35] R. Chwang, B.J. Smith, C.R. Crowell, Contact Size Effects on the Van Der Pauw Method for Resistivity and Hall Coefficient Measurement, *Solid-State Electron* 17 (1974) 1217–1227.
 - [36] K. Xing, D.L. Creedon, S.A. Yianni, G. Akhgar, L. Zhang, L. Ley, J.C. McCallum, D.-C. Qi, C.I. Pakes, Strong spin-orbit interaction induced by transition metal oxides at the surface of hydrogen-terminated diamond, *Carbon* (2020) <http://doi.org/10.1016/j.carbon.2020.03.047>
 - [37] K.E.J. Goh, M.Y. Simmons, A.R. Hamilton, Electron-electron interactions in highly disordered two-dimensional systems, *Phys. Rev. B - Condens. Matter Mater. Phys.* 77 (2008) 235410.
 - [38] J. Beheshtian, A.A. Peyghan, Z. Bagheri, Detection of phosgene by Sc-doped BN nanotubes: A DFT study, *Sensors Actuators, B Chem.* 171–172 (2012) 846–852.
 - [39] H.X. Young, Y. Yu, L.F. Xu, C.Z. Gu, Ab initio study of molecular adsorption on hydrogenated diamond (001) surfaces, *J. Phys. Conf. Ser.* 29 (2006) 145–149.
 - [40] Y. Xiang, M. Jiang, H. Xiao, K. Xing, X. Peng, S. Zhang, A DFT study of the surface charge transfer doping of diamond by chromium trioxide, *Appl. Surf. Sci.* 496 (2019) 143604.
 - [41] N. Wang, M. Li, H.Y. Xiao, X. Zu, L. Qiao, Layered LaCuOSe: A Promising Anisotropic Thermoelectric Material, *Phys. Rev. Appl.* 13 (2020) 024038.